Northumbria Research Link

Northumbria University NEWCASTLE

UniversityLibrary

Cyclic compressive behavior of limestone and silicomanganese slag concrete subjected to sulphate attack and wetting-drying action in marine environment

Matthew Zhi Yeon Ting, Kwong Soon Wong, Muhammad Ekhlasur Rahman, Meheron Selowarajoo

Matthew Zhi Yeon Ting

1) Department of Civil and Construction Engineering, Faculty of Engineering and Science, Curtin University Malaysia, CDT 250, 98009 Miri, Sarawak, Malaysia

Email: matthew.ting@postgrad.curtin.edu.my

Kwong Soon Wong (Corresponding author)

1) Department of Civil and Construction Engineering, Faculty of Engineering and Science, Curtin University Malaysia, CDT 250, 98009 Miri, Sarawak, Malaysia

Email: wongkwongsoon@curtin.edu.my

Tel: +6085 443939

Fax: +6085 443837

Muhammad Ekhlasur Rahman

1) Department of Civil and Construction Engineering, Faculty of Engineering and Science, Curtin University Malaysia, CDT 250, 98009 Miri, Sarawak, Malaysia

2) Faculty of Engineering and Environment, Northumbria University, Newcastle upon Tyne, UK

Email: merahman@curtin.edu.my

Meheron Selowarajoo

1) Department of Civil and Construction Engineering, Faculty of Engineering and Science, Curtin University Malaysia, CDT 250, 98009 Miri, Sarawak, Malaysia

Email: meheron.sj@curtin.edu.my

30 **Abstract**

31 Concrete in maritime structure is vulnerable to deterioration owing to external sulphate

32 attack, which can be exacerbated by wetting-drying action (WDA), jeopardizing its

33 resistance to cyclic loads such as wind, wave and earthquake actions. This study aims

34 to investigate the compressive fatigue behavior of concrete exposed to sulphate attack

35 and WDA in marine environment. Cyclic compressive loading test was conducted on

36 concrete after 150 days of deterioration. The effects of sulphate attack and WDA, upper

37 stress loading level and loading frequency on fatigue life, residual strain, variation of

38 elastic modulus and post-cyclic compressive strength were investigated. The sulphate

39 penetration profiles, volume change and mass change of concrete during the exposure

40 time were also measured. In addition, the performance of limestone concrete and SiMn

41 slag concrete was compared in the study. The sulphate ion was found to penetrate

42 concrete up to a depth of 20 mm, with a maximum content of 1.72% to 2.58% near the

43 surface. The cyclic loading test showed that degraded concrete had 38.2% higher

44 residual displacement and 1.4% lower modulus of elasticity than normal concrete. The

45 sulphate attack and WDA weakened the concrete, reducing its fatigue resistance. SiMn

46 slag concrete had a lower fatigue life, larger residual displacement and greater stiffness

47 degradation than limestone concrete.

48

49 Keywords: Sulphate attack, Wetting-drying cycles, Fatigue life, Residual displacement,

50 Silicomanganese slag

51

1. Introduction

Concrete, a versatile and economical building material, has been broadly used in maritime structures such as berthing, docking and coastal defense infrastructure [1]. In hostile marine environment, concrete is vulnerable to material deterioration caused by the seawater and weathering. Seawater generally contains significant levels of chloride, sulphate and carbon dioxide, all of which can imperil concrete through chloride-induced corrosion, sulphate attack and carbonation [2]. Chloride attack destroys the protective film of steel reinforcement, leading to steel corrosion [3]. Carbon dioxide reacts with calcium components in concrete which depletes the portlandite, reducing the concrete alkalinity and hence causing the loss of corrosion resistance of embedded steel [4]. Both chloride attack and carbonation bring about corrosion issue in reinforced concrete. Meanwhile, sulphate attack is a more severe threat to the durability of concrete because it causes hydrate dissolution, damage due to formation of expansive products and strength reduction, affecting the performance of both mass concrete and reinforced concrete [5]. Therefore, this research work, which aims to evaluate the performance of plain concrete, focuses on the concrete deterioration mechanism of external sulphate attack.

Sulphate attack occurs when the sulphate ion from saline environment reacts with aluminate hydrate and calcium hydroxide in concrete to form expansive products of ettringite and gypsum [6]. Extensive researches have been conducted to study the chemical reaction [7, 8], expansion mechanism [9, 10] and mechanical response [11] in concrete subjected to sulphate attack. The study was then extended to incorporate the influence of environmental factor of wetting-drying action (WDA) on concrete deterioration. In wetting and drying environment, the sulphate attack led to more severe damage due to the increased capillary absorption [5, 12]. In addition, the WDA also

77 induced drying shrinkage and salt crystallization to damage concrete, resulting in

78 micro-cracking [13]. Nonetheless, Wu et al. [14] found that the crack could be partially

79 restored during the concrete rewetting. The increased permeability of damaged concrete

80 could be reduced by the most 50%, when the cement matrix absorbed water and swelled

81 to close the fracture.

82 The effect of external loading in combination with WDA on sulphate attack has also

83 been investigated in order to replicate the actual in-service condition of concrete. Gao

84 et al. [15] demonstrated that applying flexural loading and WDA to concrete at the same

85 time resulted in more severe damage in sulphate attack. The flexural loading caused

86 tensile strain to enlarge concrete pore and increase the ingress of sulphate ion,

87 accelerating concrete deterioration [13]. Chen et al. [16] found that long-term loading

88 produced more severe damage than short-term loading since the former resulted in

89 irreversible concrete creep under the sustained load. In marine environment, concrete

90 structures are frequently subjected to cyclic loads caused by wind, wave and earthquake.

91 Sulphate attack and WDA degrade concrete performance, particularly the mechanical

92 property, which may reduce its resistance to cyclic loading. To date, limited research

93 has been conducted on the concrete deterioration caused by the synergy of cyclic

94 loading, sulphate attack and WDA. Therefore, the aim of this research is to evaluate the

95 fatigue behavior of concrete after the deterioration caused by sulphate attack and WDA.

96 Cyclic loading is a series of load repetitions that can be constant or varying in loading

97 magnitude and frequency. Although the applied load is lower than compressive strength,

98 concrete exposed to cyclic loading can still experience a progressive material damage

99 such as micro-cracking and stiffness reduction [17]. Concrete fatigue strength is defined

100 as stress limit that concrete can endure for a given number of cycles before failure. The

101 fatigue strength of concrete in the structural design is limited to 60% of the design

102   strength [18]. Cyclic loading can be categorized into two types, low-cycle and high-

103   cycle loadings. Low-cycle loading is the situation when fewer loading cycles are

104   applied, but with higher stress. ACI 215R-74 specifies the low-cycle fatigue as concrete

105   failure within 1×10^2 cycles of applied load [19]. The failure is usually caused by high

106   stress loading such as earthquake. On the other hand, high-cycle fatigue refers to the

107   loading condition with high number of cycles at a low stress level. High-cycle fatigue

108   is caused by traffic load and wind action. The failure typically occurs after subjected to

109   1×10^2 to 1×10^7 cycles of loading [17]. The fatigue strength of concrete can be reduced

110   by the maritime deterioration mechanism. In this context, consideration of cyclic

111   loading is also an important aspect of the study of concrete performance in marine

112   environment.

113   Concrete cyclic loading test is generally conducted for various loading arrangements

114   such as compression, tension and bending. The commonly used fatigue test is the

115   flexural test due to simple set-up and popular application. Past researches have

116   investigated the flexural loading of concrete in combination with sulphate attack and

117   WDA [20, 21]. However, limited research on cyclic loading test under compression has

118   been conducted. In this context, this research aims to evaluate the compressive fatigue

119   behavior of concrete exposed to sulphate attack and WDA. In the experiment, sulphate

120   ion penetration profile, mass change and volume change of concrete are measured

121   throughout the period of exposure to sulphate attack in wetting and drying environment.

122   Cyclic compressive loading test is carried out on the concrete after 150 days of sulphate

123   attack and WDA. In the cyclic loading test, the effects of sulphate attack and WDA,

124   upper stress loading level and loading frequency on fatigue life, residual strain,

125   variation of elastic modulus and post-cyclic compressive strength are studied.

126   Furthermore, the performance of limestone concrete and SiMn slag concrete subjected

127 to sulphate attack and WDA is also compared in the study. This research intends to

128 develop concrete for use in mass concrete, particularly for breakwater amour, where

129 steel reinforcement is not used. Therefore, concrete performance related to steel

130 reinforcement corrosion is not taken into account in this study.

131 **2. Experimental program**

132 *2.1.   Materials*

133 Ordinary Portland cement with a grade of 42.5 N manufactured by Cahaya Mata

134 Sarawak in Malaysia was used in this investigation. Supplementary cementitious

135 materials, including fly ash (FA) from Mukah Power Generation Sdn. Bhd. coal-fired

136 power plant and silica fume (SF) from Novakey Developers Sdn. Bhd., were used to

137 partially replace cement. Table 1 shows the main oxide contents of cement, FA and SF.

138 Limestone with a specific gravity of 2.64 was used as coarse aggregate. For comparison

139 purpose, SiMn slag with specific gravity of 2.97 was also used to fully replace

140 limestone in some concrete mixtures. A mixture of marine sand and quarry dust with

141 fineness modulus of 2.59 and specific gravity of 2.7 was used as fine aggregate. Table

142 2 presents the particle size grading and physical properties of the aggregates. The

143 aforementioned materials were mixed with seawater. The effect of seawater on concrete

144 properties has been investigated previously [22, 23], hence it is not discussed further in

145 this study. In addition, sodium naphthalene sulphonate formaldehyde, a Type A (water-

146 reducing) chemical admixture specified by the ASTM C494 standard, was used as to

147 ensure sufficient concrete workability [24].

148

Table 1: Oxide contents of cement, fly ash and silica fume [23]

Oxide	CaO	SiO$_2$	Al$_2$O$_3$	Fe$_2$O$_3$	MgO	SO$_3$	K$_2$O	Na$_2$O
Cement (%)	70.0	16.3	4.2	3.5	1.7	1.4	1.0	0.1
Fly ash (%)	18.9	38.9	13.4	15.7	4.0	1.8	2.5	2.1
Silica fume (%)	0.1	96.2	-	0.2	0.5	0.9	0.3	0.1

Table 2: Particle size distribution and physical property of aggregate [22, 23]

Particle size (mm)	Cumulative passing (%)		
	Limestone	SiMn slag	Marine sand mixture
37.5	-	100	-
25	100	33.7	-
19	92.6	28.2	-
12.5	87.5	8.5	-
9.5	32.3	4.8	-
4.75	12.1	0	100
2.36	0	-	95.1
1.18	-	-	80.7
0.6	-	-	70.9
0.3	-	-	31.7
0.15	-	-	3.2
0.075	-	-	0
Water absorption (%)	0.66	0.21	-
Flatness ratio	0.68	0.55	-
Elongation ratio	0.68	0.59	
Abrasion resistance (%)	12	22	-

2.2.   Concrete mix proportions

Table 3 summarizes the concrete mix proportion designed using Absolute Volume Method in accordance with the ACI 211.4R-08 standard [25]. Four types of concrete were included to assess the performance of concrete subjected to sulphate attack and WDA. The first two concrete mixes used limestone as coarse aggregate and were abbreviated as LS (C) and LS (SF-FA). LS (C) represented control mix and LS (SF-FA)

159 represented concrete containing FA and SF. The replacement levels of FA and SF were

160 16.3% and 11.5% respectively, based on the optimization performed by Ting et al. [23].

161 In addition, two types of SiMn slag concrete with similar FA and SF contents to

162 limestone concrete were also included for comparison. The SiMn slag concrete was

163 abbreviated as SiMn (C) and SiMn (SF-FA). For all the mixes, the water-to-binder

164 (W/B) ratio was kept constant at 0.32. The SP dosage was 1% of the total binder content.

165 The workability of each concrete mix has been determined by slump test and the results

166 are shown in Table 3.

167

Table 3: Concrete mix proportion

Materials	Mix proportion (kg/m^3)			
	LS (C)	LS (SF-FA)	SiMn (C)	SiMn (SF-FA)
Cement	550	406	550	406
Fly ash	0	54	0	54
Silica fume	0	90	0	90
Limestone	965	965	0	0
SiMn slag	0	0	1115	1115
Marine sand	515	501	515	501
Quarry dust	173	168	173	168
Water	176	176	176	176
Superplasticizer	5.5	5.5	5.5	5.5
Slump value (mm)	90	125	75	106

168

169 *2.3.   Experimental details*

170 *2.3.1.   Wetting and drying of concrete specimen*

171 To reduce the effect of hydration on test results, all concrete specimens were fully

172 submerged in water after casting and demoulding until they reached 165 days of age.

173 The concrete specimens were transferred to plastic containers for cyclic wetting-drying

174 and sulphate immersion test. The wetting-drying process consisted of immersing the

specimen in salt solution for 12 hours and drying them in the air at 27±1 °C for 11 hours. The test procedure took 45 minutes to drain the salt solution and 15 minutes to fill the container. Therefore, the duration of one complete wetting-drying cycle was 24 hours. The salt solution used in the wetting stage was prepared by dissolving the chemical grade sodium sulphate (Na_2SO_4) powder in water. Na_2SO_4 solutions with two different concentrations were used, namely 5wt% (Exposure I) and 20wt% (Exposure II). The solution was freshly replaced every 30 days. In addition, specimens were also treated by fully immersing them in salt solution and tap water for comparison. Two types of solution, 20wt% Na_2SO_4 solution (Exposure III) and tap water (Exposure C), were used.

2.3.2. *Sulphate ion penetration profile test*

Concrete prism with a dimension of 75 x 75 x 300 mm was used in the sulphate ion profile test. The sulphate ion intrusion profile was determined by measuring the distribution of SO_4^{2-} ions from the surface to the interior of the concrete. After 90 days and 150 days of exposure to sulphate attack, powder samples were collected from the concrete specimen by drilling at several points along the ingress path. The samples were obtained from four penetration depths, which ranged from 0 to 5 mm, 5 to 10 mm, 10 to 15 mm and 15 to 20 mm, with the average depths of 2.5, 7.5, 12.5 and 17.5 mm respectively as shown in Figure 1. The SO_4^{2-} ion content of the powder sample was determined using the barium sulphate gravimetric method in accordance with the ASTM C114 standard [26]. Table 4 shows the initial SO_4^{2-} ion contents of concrete for each mix, which were determined prior to sulphate attack.
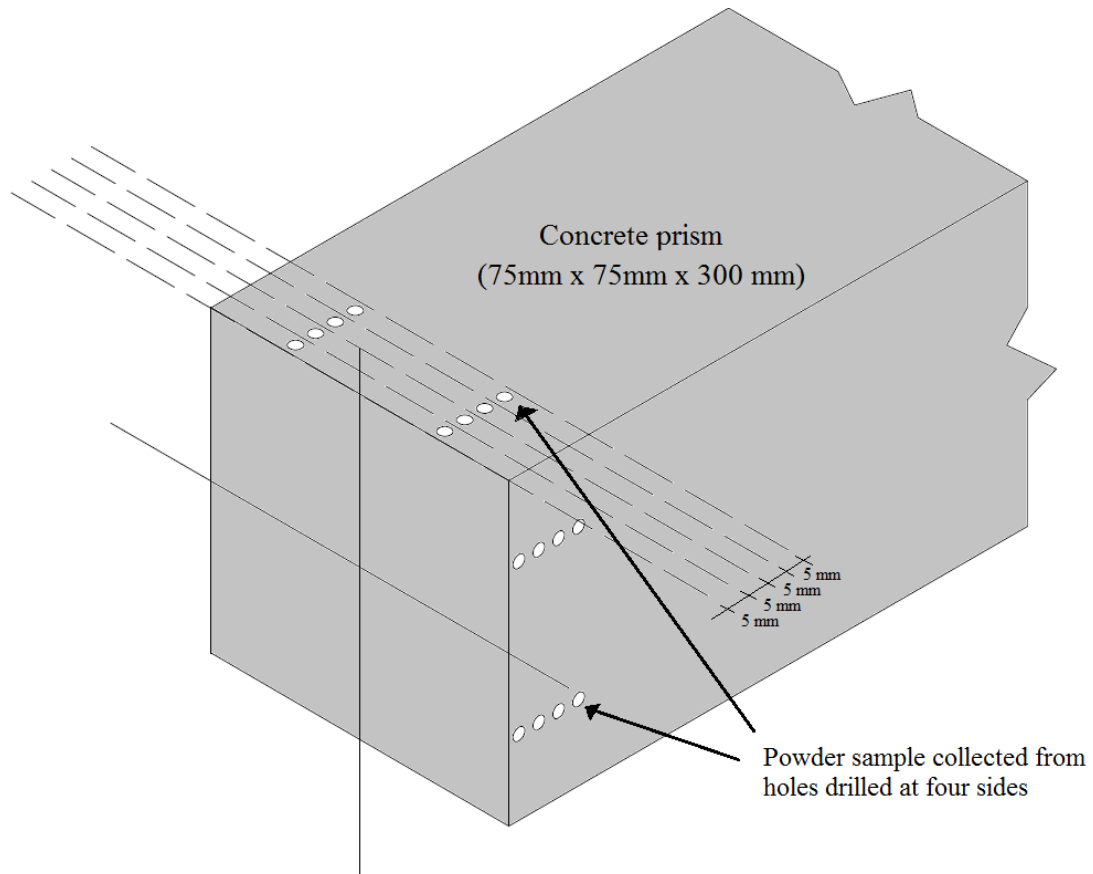
197 **Table 4: Initial SO$_4^{2-}$ ion content of concrete**

Concrete Mix	Inition SO$_4^{2-}$ content (%)
LS (C)	0.41
LS (SF-FA)	0.28
SiMn (C)	0.48
SiMn (SF-FA)	0.31

198

200 **Figure 1: Powder sample collection from concrete prism**

201

202 *2.3.3.   Mass and volume change of concrete*

203 Concrete experienced changes in mass and volume due to the deterioration caused by

204 sulphate attack and WDA. The test was conducted in accordance with test method

205 specified by ASTM C1012 standard [27]. Concrete prisms 75 x 75 x 300 mm were used

206 for the measurement of changes in mass and volume. The change in mass and volume

207 was determined using Equation 1 and Equation 2. Both mass and volume changes were

208 determined after 30, 60, 90, 120 and 150 days of exposure.

$$\Delta m_t = \frac{m_o - m_t}{m_o} \times 100\% \qquad \qquad \text{Equation 1}$$

$$\Delta v_t = \frac{v_o - v_t}{v_o} \times 100\% \qquad \qquad \text{Equation 2}$$

209 In the equations, Δm_t and Δv_t are the mass and volume change of concrete at the

210 respective exposure time, m_o and v_o are the mass and volume of concrete before the

211 exposure, and m_t and v_t are mass and volume of concrete measured at the respective

212 exposure period.

213 *2.3.4.   Cyclic loading test*

214 The cyclic compressive loading test for concrete was performed on 50 mm cube

215 specimens using a 100 kN Instron Universal Testing Machine 5982 as shown in Figure

216 2. Table 5 shows the specimen details for cyclic loading test. In the test, the lower stress

217 level (S_{min}) was set constant at 1% of the static compressive strength of concrete. The

218 upper stress levels (S_{max}) studied in the investigation were 30%, 40%, 45%, 80%, 85%

219 and 90% of compressive strength. The loading frequencies investigated were 0.6, 0.8

220 and 1 Hz. The specimens were labelled as Tx-Sy-Fz, with "T" referring to the type of

221 concrete mix exposed to particular condition, "S" referring to the upper stress level and

222 "F" referring to the loading frequency, as shown in Table 5. For example, T2-S0.9-F0.8

223 indicated SiMn (SF-FA) concrete exposed to 150 days of WDA in 20% Na_2SO_4

224 solution, and was tested using 90% compressive strength as S_{max} at a loading frequency

225 of 0.8 Hz. Three specimens from each type of concrete were tested.

226 The average static compressive strength of concrete specimens was first determined

227 and this value was used as input for the cyclic loading test. Before the cyclic loading

test, concrete specimen was pre-loaded at 5 kN for 2 minutes to flatten the loading

surface. The force and displacement of the specimen in vertical direction were recorded

using the loading cell and extensometer respectively. The test was terminated after

10,000 loading cycles if the specimen did not fail. The compressive strength of the

intact specimen was then tested.

Table 5: Detail of specimen in cyclic loading test

| Series	Notation	S_{max}	S_{min}	Loading frequency (Hz)	Number of specimen	Concrete mix	Exposure condition
Series 1	T1	1	-	-	3	SiMn (SF-FA)	Exposure C for 150 days
	T1-S0.3-F0.8	0.3	0.01	0.8	3		
	T1-S0.4-F0.8	0.4	0.01	0.8	3		
	T1-S0.45-F0.8	0.45	0.01	0.8	3		
	T1-S0.45-F0.6	0.45	0.01	0.6	3		
	T1-S0.45-F1.0	0.45	0.01	1.0	3		
Series 2	T2	1	-	-	3	SiMn (SF-FA)	Exposure II for 150 days
	T2-S0.45-F0.8	0.45	0.01	0.8	3		
	T2-S0.8-F0.8	0.8	0.01	0.8	3		
	T2-S0.85-F0.8	0.85	0.01	0.8	3		
	T2-S0.9-F0.8	0.9	0.01	0.8	3		
Series 3	T3	1	-	-	3	LS (SF-FA)	Exposure II for 150 days
	T3-S0.8-F0.8	0.8	0.01	0.8	3		
	T3-S0.85-F0.8	0.85	0.01	0.8	3		
	T3-S0.9-F0.8	0.9	0.01	0.8	3		
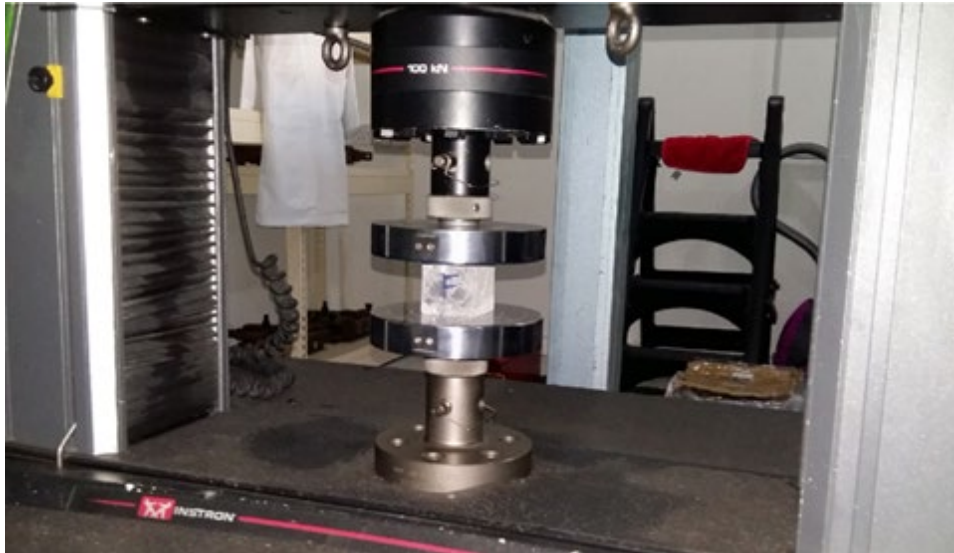
Figure 2: Cyclic compressive loading test set-up

3. Results and discussion

3.1.   Sulphate ion penetration profile

The initial sulphate (SO_4^{2-}) ion content of concrete for all mixes prior to the test has been determined and is shown in Table 4. All concrete contained a low amount of initial SO_4^{2-} ion, ranging from 0.28% to 0.48%. The initial SO_4^{2-} ion content in the concrete was produced by the hydration of cement. The partial replacement of cement by FA and SF could slightly reduce the initial SO_4^{2-} ion content. In the following section, the initial SO_4^{2-} ion content was deducted from the measured SO_4^{2-} ion value in the sulphate ion penetration profile of concrete.

Figure 3 shows the sulphate ion penetration profile of all types of concrete after 150 days of exposure to WDA in 20% Na_2SO_4 solution (Exposure II). The SO_4^{2-} ion content decreased with an increase in depth towards the interior of concrete. The SO_4^{2-} ion content was 1.72%–2.58%, 0.73%–1.23% and 0.4%–0.57% at the average depth of 2.5 mm, 7.5 mm and 12.5 mm respectively. At an average depth of 17.5 mm, all concrete

253   mixes had a SO_4^{2-} ion content of less than 0.5%. SiMn (C) had the highest SO_4^{2-} ion

254   content along the depth of penetration. The incorporation of FA and SF improved the

255   concrete resistance to sulphate penetration. The effect of FA and SF was also shown in

256   limestone concrete, where the SO_4^{2-} ion contents of LS (SF-FA) reduced by 0.41%

257   compared to LS (C) at 2.5 mm depth. The findings were in line with those of Qi et al.

258   [28] who found better sulphate resistance if the concrete was incorporated with ground

259   granulated blast furnace slag (GGBFS) and FA. The use of supplementary cementitious

260   materials enhanced the concrete pore structure and improved its resistance against

261   sulphate intrusion.

262   Besides, the SO_4^{2-} ion content of limestone concrete was typically lower than that of

263   SiMn slag concrete. The higher sulphate concentration of SiMn slag concrete was due

264   to the weaker bonding of SiMn slag aggregate with cementitious matrix. The SiMn slag

265   aggregate was angular and had a smoother surface than limestone aggregate. Zhang et

266   al. [29] also found that the weaker aggregate bonding of recycled aggregate concrete

267   resulted in an increased intrusion of sulphate. Nonetheless, the difference in SO_4^{2-} ion

268   content between the concrete mixes decreased with the increasing depth of concrete.
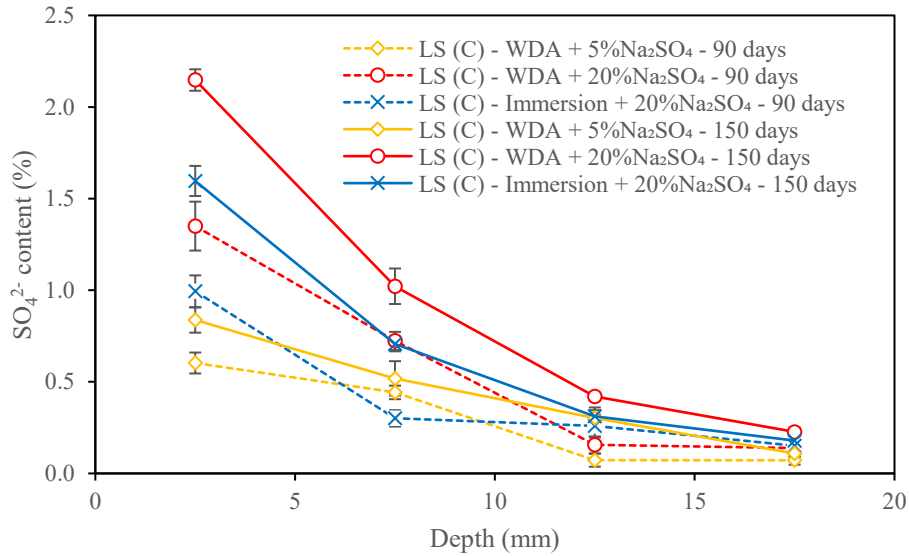
269   The sulphate profile of LS (C) exposed to 90 and 150 days of three exposure conditions,

270   namely WDA in 5% Na_2SO_4 solution (Exposure I), WDA in 20% Na_2SO_4 solution

271   (Exposure II) and full immersion in 20% Na_2SO_4 solution (Exposure III), is shown in

272   Figure 4. The SO_4^{2-} ion content along the concrete depth increased with the exposure

273   time. For instance, SO_4^{2-} ion content of LS (C) was 1.35% at depth 0–5 mm after 90

274   days in Exposure II. At 150 days, the SO_4^{2-} ion content increased to 2.15% for the same

275   depth. The increment was due to the diffusion of SO_4^{2-} ion caused by concentration

276   gradient and the capillary absorption. The sulphate attack also damaged the concrete,

277   causing cracks and leading to a more penetration of SO_4^{2-} ion [30].

14

278   The SO_4^{2-} ion content of concrete in Exposure II was approximately two times higher

279   than that in Exposure I. This was due to the higher concentration of Na_2SO_4 solution

280   used in Exposure II, but the increment was not directly proportional to the increase in

281   solution concentration. A higher solution concentration produced a greater amount of

282   expansive components such as ettringite and gypsum, which filled up the concrete pore

283   and slightly slowed down the sulphate penetration [31]. By comparing the Exposure II

284   and Exposure III, the WDA increased the SO_4^{2-} ion content by approximately 1.3 times.

285   The cyclic behavior of WDA accumulated the SO_4^{2-} ion at the wetting front, which

286   induced higher concentration gradient for greater diffusion [32].
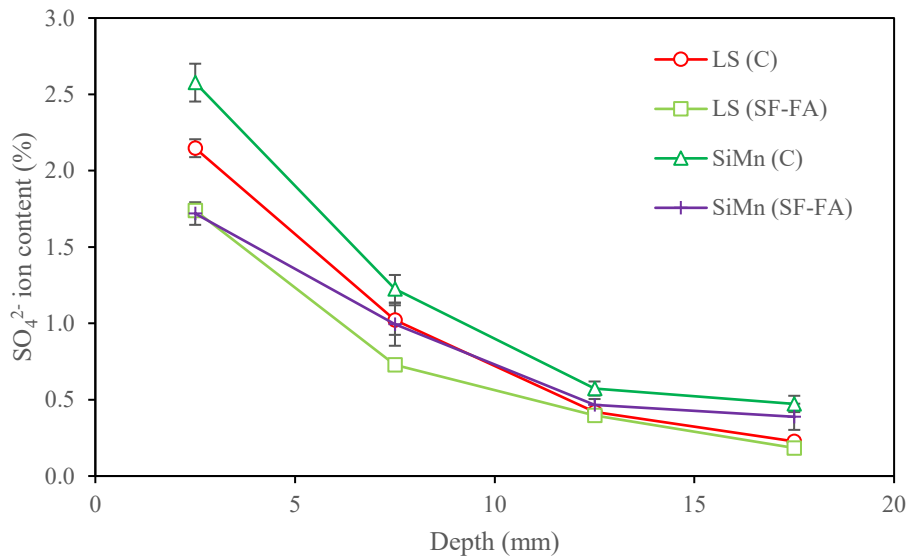
287

288 **Figure 3: SO_4^{2-} ion penetration profile of concrete exposed 150 days of WDA in**
289 **20% Na_2SO_4 solution (Exposure II)**

**Figure 4: SO$_4^{2-}$ ion penetration profile of LS (C) exposed to 90 and 150 days of various sulphate attack conditions**

3.2. Mass change of concrete

The mass change of concrete with exposure time was also measured. Figure 5 shows the mass change of all concrete exposed to WDA in 20% Na$_2$SO$_4$ solution (Exposure II). The concrete experienced two stages of mass change, an increasing stage and a decreasing stage. Both SiMn (C) and LS (C) exhibited a similar trend of mass change. The mass of both concrete types increased by 0.43% and 0.42% at 60 days, but they decreased to -0.49% and -0.39% at 150 days. Jiang and Niu [5] also observed a two-stage mass change for concrete exposed to WDA in various types of sulphate solution. The mass gain was due to the formation of ettringite and gypsum inside concrete pores. However, at the later stage, the accumulation of these expansive products exerted stress to damage the concrete, leading to the mass loss. The surface damage, such as spalling of mortar layer due to shrinkage during the drying period, also resulted in the mass loss [31].

307 SiMn (SF-FA) and LS (SF-FA), which contained FA and SF, did not undergo a mass-

308 decreasing stage of up to 150 days. The addition of FA and SF enhanced the pore

309 structure of concrete and reduced the intrusion of sulphate. The pozzolanic reaction of

310 FA and SF also improved the mechanical property of concrete and the resultant concrete

311 had a higher resistance to sulphate attack and WDA. The results related well to the

312 research of Qi et al. [28] who found a constant mass gain in concrete containing GGBS

313 and FA for up to 270 days.

314 Figure 6 compares the mass change of LS (C) exposed to three types of exposure

315 environment, namely WDA in 5% Na_2SO_4 solution (Exposure I), WDA in 20% Na_2SO_4

316 solution (Exposure II) and full immersion in 20% Na_2SO_4 solution (Exposure III). From

317 0 to 90 days, the mass of concrete in Exposure I gradually increased and then became

318 constant, with no noticeable mass-decreasing stage. The maximum mass gain in

319 Exposure I was 0.28% lower than that in Exposure II. The greater mass gain of concrete

320 in Exposure II was attributed to a higher concentration of sulphate solution, which

321 increased the formation of ettringite and gypsum and accelerated concrete deterioration.

322 On top of that, the mass change of concrete in Exposure III had a similar result trend to

323 that in Exposure II, but with at a lower rate. The difference was particularly evident at

324 the mass-decreasing stage. At 150 days, the mass loss for Exposure III was 0.32% less

325 than that of Exposure II. This indicated that the WDA had a significant effect on the

326 aggravation of sulphate attack. The wetting and drying cycle increased the penetration

327 of sulphate and induced salt crystallization to exacerbate the deterioration.
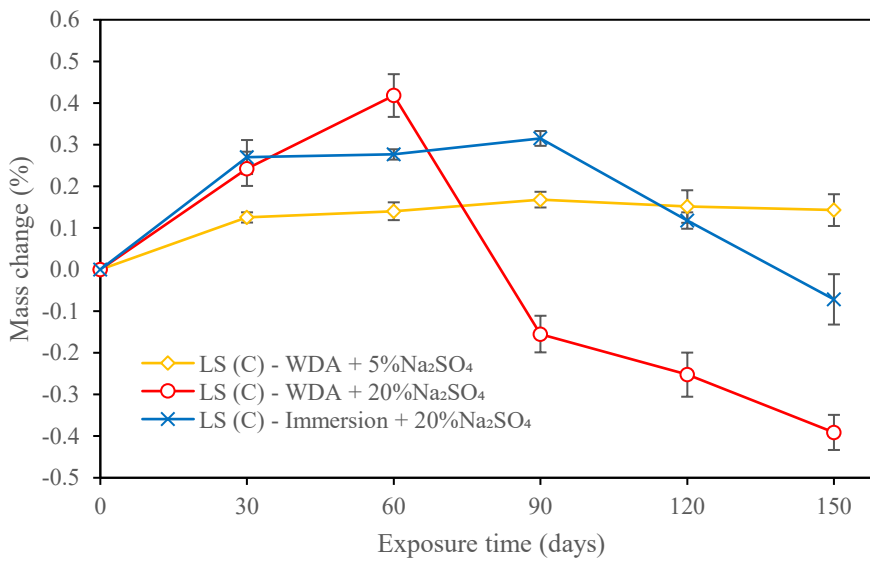
328

329
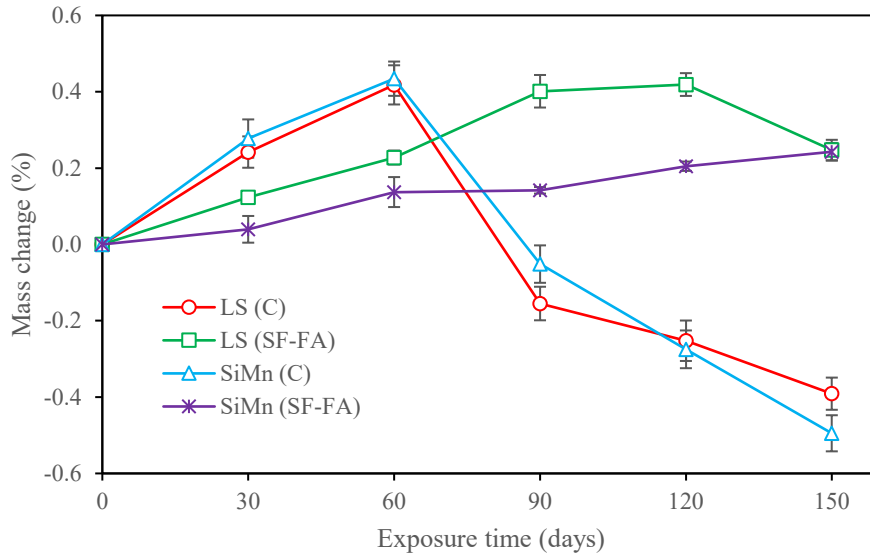
Figure 5: Mass change over time for concrete exposed to WDA in 20% Na$_2$SO$_4$ solution (Exposure II)

332

333

Figure 6: Mass change over time for LS (C) exposed to various sulphate attack conditions

336

3.3.   Volume change of concrete

In addition to mass change, concrete experienced swelling and expansion as a result of sulphate attack. Figure 7 shows the volume change of concrete for all mixes after 150 days of exposure to WDA in 20% Na_2SO_4 solution (Exposure II). The volume of concrete increased gradually over the exposure time. The expansion was minimal at the early exposure time, but was more evident at a later stage. For example, the concrete volume increased by 0.27% –0.4% at 60 days, and it increased by 0.73%– 1.23% at 150 days. The expansion was due to the formation of expansive products such as ettringite and gypsum caused by sulphate attack [30]. The lower expansion rate during the early stage was due to the filling up of concrete pores by these products. But, a further accumulation of ettringite and gypsum caused the concrete to expand at the later stage.

Limestone concrete expanded more than SiMn slag concrete in the early stage, but less in the later stage. The expansion of LS (C) and LS (SF-FA) concrete was 0.15% and 0.13%, respectively, more than that of SiMn (C) and SiMn (SF-FA) concrete at 30 days. At 150 days, however, the expansion of limestone concrete was 0.14% and 0.07%, respectively, less than that of SiMn slag concrete. This was attributed to the lower compressive and tensile strengths of SiMn slag concrete in resisting expansion. But, at the early stage, the weaker bonding of SiMn slag aggregate with cement paste resulted in more concrete pores, providing space for the accumulation of expansive products. As shown in the SEM images in Figure 9, SiMn (SF-FA) had more pores compared to LS (SF-FA). Qi et al. [28] also found that recycled aggregate concrete was more porous than normal concrete, which experienced more expansion. Nevertheless, both concrete still had a good and strong bonding between cement paste and aggregate, as the interfacial transition zone was not apparent. Besides, the results in Figure 7 showed that the addition of FA and SF reduced concrete expansion. FA and SF strengthened the

mechanical property of concrete to resist the expansion. The refinement of pore structure by FA and SF also reduced the permeability of concrete, minimizing the penetration of sulphate ion. Zhongya et al. [12] demonstrated that the expansion of FA concrete and SF concrete was 1.3% and 1.2%, respectively, lower than that of control concrete.

Figure 8 shows the volume expansion of LS (C) concrete exposed to different exposure conditions, including WDA in 5% Na_2SO_4 solution (Exposure I), WDA in 20% Na_2SO_4 solution (Exposure II) and immersion in 20% Na_2SO_4 solution (Exposure III). The volume expansion of concrete in Exposure I ranged from 0.01% to 0.45% during the period from 30 to 150 days. The expansion was lower than that of concrete in Exposure II, where it ranged from 0.22% to 1.09% over the same period. The use of salt solution with a higher sulphate concentration accelerated the damage process. The expansion of concrete in Exposure III was less than that in Exposure II, but higher than that in Exposure I. The expansion of concrete exposed to WDA was approximately 1.5 times higher than that of concrete subjected to full immersion in sulphate solution with the same concentration. The result was consistent with that reported by Yu et al. [33], who showed that WDA caused a two-fold volume expansion relative to concrete that was completely submerged in salt solution. Apart from the increased sulphate penetration rate, the WDA also induced salt crystallization, which caused expansion.
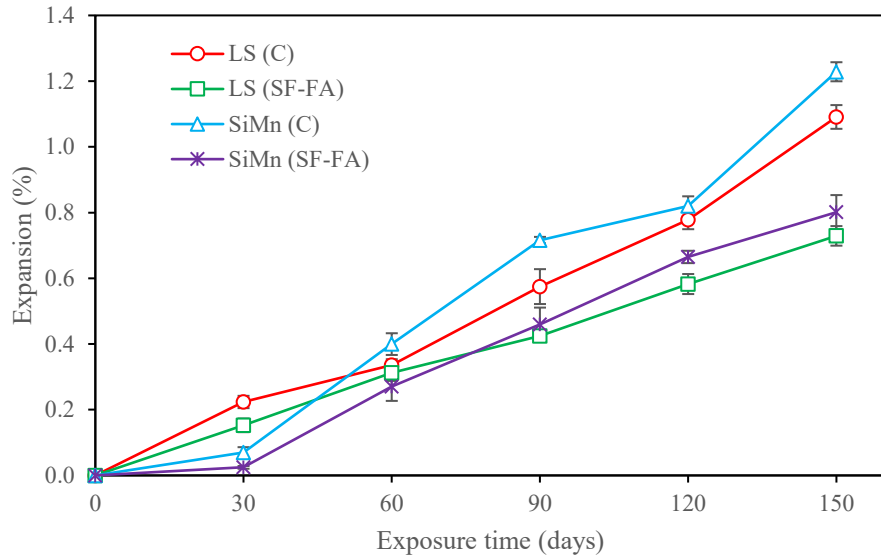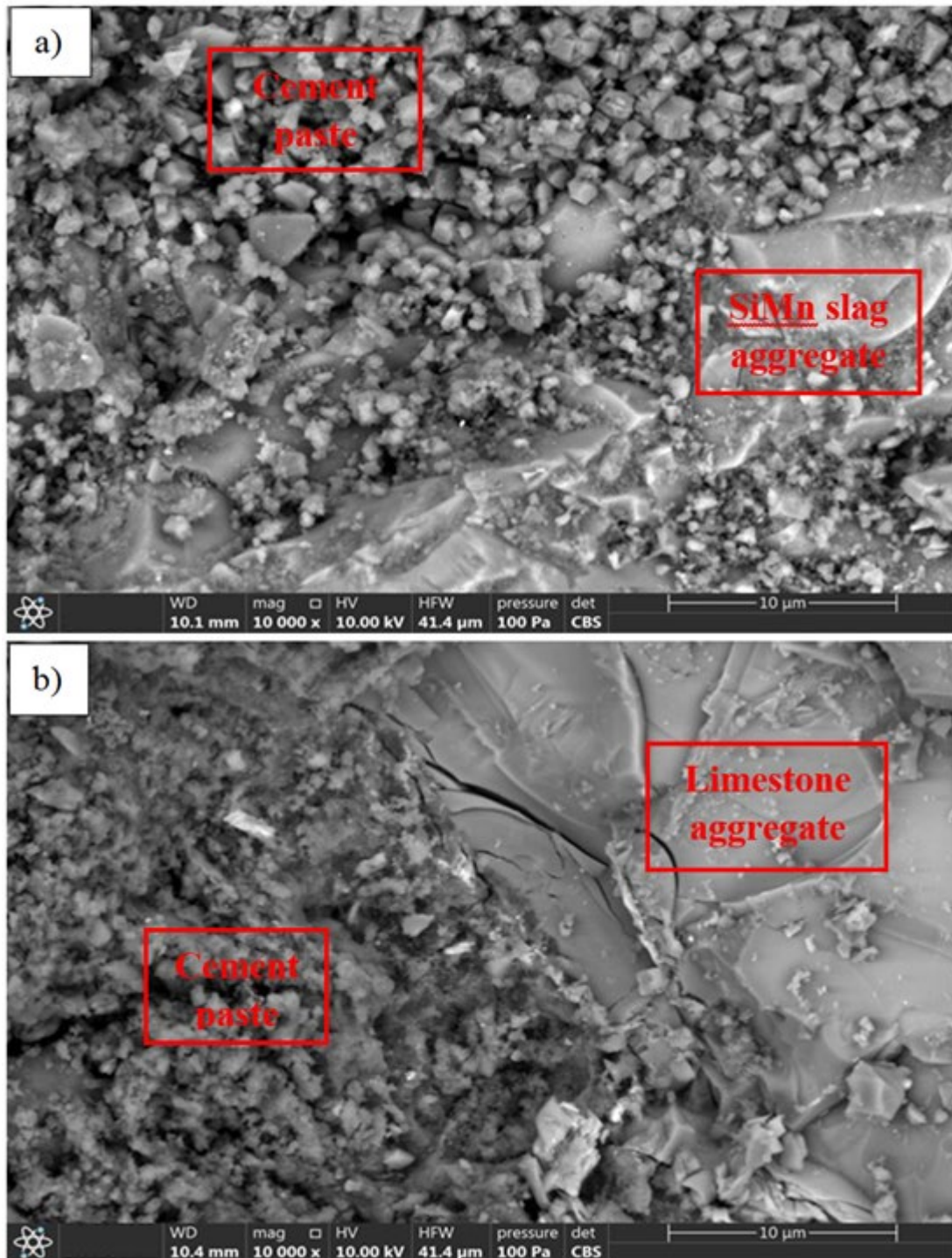
Figure 7: Expansion of concrete exposed to WDA in 20% Na₂SO₄ solution (Exposure II)
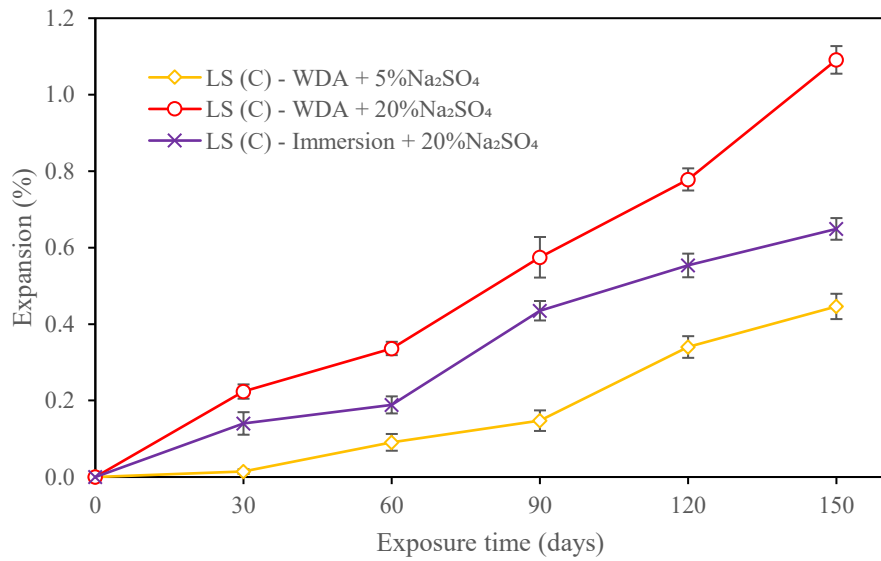
Figure 8: Expansion of LS (C) exposed to various sulphate attack conditions

Figure 9: SEM image of (a) SiMn (SF-FA) and (b) LS (SF-FA) after 165 days of water curing and 150 days of full immersion in water

391 *3.4. Compressive strength under static loading*

392 The compressive strength of concrete under static loading has been determined using

393 50 mm cubic specimens and the results are shown in Table 6. T1 was SiMn (SF-FA)

394 specimen that had been fully submerged in tap water (Exposure C) for 150 days. T2

395 and T3 were respectively SiMn (SF-FA) and LS (SF-FA) specimens exposed to WDA

396 in 20% of Na_2SO_4 solution (Exposure II) for 150 days. The average compressive

397 strength of T1, T2 and T3 was measured as 91.37 MPa, 40.98 MPa and 45.86 MPa,

398 with a standard deviation of 1.02 MPa, 2.16 MPa and 2.21 MPa respectively. The

399 standard deviation of T2 and T3 was higher than that of T1. This was attributed to the

400 inconsistent deteriorating effect of the sulphate attack and WDA and inhomogeneous

401 property of concrete [31]. The irregular defects in concrete specimen had resulted in

402 the higher variance in compressive strength.

403 The specimen size effect was also studied by comparing the compressive strength of 50

404 mm cube to 100 mm cube as shown in Table 6. According to Del Viso et al. [34], the

405 compressive strength of concrete generally decreased with an increase in cube size due

406 to the presence of more flaws in larger cube. However, T1 had a compressive strength

407 slightly lower than that of 100 mm cube, with a ratio of 0.97. This was due to the

408 relatively larger coarse aggregate used in the manufacture of 50 mm cube, which had a

409 negative effect on the homogeneity of concrete. Fladr and Bily [35] also found that the

410 minimum relative strength between a 100 mm cube and a 50 mm cube was 0.9.

411 Following the sulphate attack and WDA, the relative strength of T2 and T3 was further

412 reduced to 0.64 and 0.68 respectively, indicating a more severe deterioration of the

413 smaller specimen. Based on the sulphate ion profile determined in previous section, the

414 depth of concrete that was affected by the sulphate attack was up to 20 mm. Under a

three-dimensional intrusion of sulphate, the 50 mm cube was almost completely
deteriorated by the sulphate attack and WDA, leading to greater concrete damage.

Table 6: Concrete compressive strength of 50 mm cube under static loading

Series	Specimen	Compressive strength, f_c (MPa)			Strength relative to 100 mm cube
		Measured	Mean	Standard deviation	
Series 1	T1-1	90.05	91.37	1.02	0.97
	T1-2	91.54			
	T1-3	92.52			
Series 2	T2-1	38.21	46.64	2.16	0.64
	T2-2	40.26			
	T2-3	43.46			
Series 3	T3-1	42.96	45.86	2.21	0.68
	T3-2	46.31			
	T3-3	48.32			

3.5.   Fatigue life of concrete

The fatigue life (N_f) of all concrete specimens has been determined and presented in
Table 7. At the low upper stress level (S_{max}), such as 30%, 40% and 45% of compressive
strength (f_c), the specimens did not fail after 10,000 cycles of loading. Further cyclic
loading was required in order for the concrete to fail, but it was not carried out due to
time and cost constraints. Nevertheless, the behavior of these specimens with respect
to deformation and elasticity of concrete is elaborated in Section 3.6 and Section 3.7.
The failure of specimen occurred when the upper stress level was greater than 80% of
compressive strength. As shown in Table 7, the fatigue life pattern of these specimens
was inconsistent and widely distributed due to their inhomogeneous properties and high
sensitivity to experimental set-up and loading conditions. The analysis of this type of
result can be carried out using the S-N curves [36]. The S-N curves for T2 and T3

specimens are depicted in Figure 10. The fatigue life of concrete decreased with the increase in the upper stress level. This was ascribed to more rapid development of crack at a stress level which was close to the compressive strength of concrete. The finding was consistent with that of Humme et al. [37] who found that the fatigue life of specimen using S_{max} of 0.7 was greater than that of specimen using S_{max} of 0.8. The equation showing the relationship between S_{max} and N_f has been developed as Equation 3 for T2 and Equation 4 for T3. The coefficient of determination (R^2) for Equation 3 and Equation 4 is 0.9428 and 0.8789 respectively.

$$S_{max} = -0.0568\log N_f + 1.0221; \quad R^2 = 0.9428 \qquad \text{Equation 3}$$

$$S_{max} = -0.0529\log N_f + 1.0172; \quad R^2 = 0.8789 \qquad \text{Equation 4}$$

The regression equation for T2 was slightly lower than that for T3, indicating a lower fatigue life of T2 under constant stress level. The descending slope of T2 equation was also steeper than that of T3. It should be noted that at high stress level, S_{max} of 0.9, the effect of SiMn slag on fatigue life was not obvious. The fatigue strength corresponding to a fatigue life of 1 million loading cycles was $0.681 f_c$ for T2 and $0.700 f_c$ for T3, where f_c referred to compressive strength of concrete. This indicated a weaker resistance of T2 against fatigue loading. This was due to the weaker and more brittle properties of SiMn slag aggregate in T2 concrete. As shown in Table 2, SiMn slag aggregate had lower abrasion resistance than the limestone aggregate. Furthermore, SiMn slag aggregate was flakier and had a higher slenderness ratio than limestone aggregate, resulting in concrete with lower dynamic resistance. Wu and Jin [36] found that the concrete incorporated with demolished concrete lump (DCL) as coarse aggregate had a lower fatigue strength than normal concrete. Since the DCL aggregate had a lower mechanical property, the resulting concrete had a lower fatigue resistance.

**Table 7: Fatigue life (N$_f$) of concrete specimens**

Series	Specimen	Fatigue life, N$_f$ (cycles)	Specimen	Fatigue life, N$_f$ (cycles)
Series 1	T1-S0.3-F0.8-1	10,000 (Not failed)	T1-S0.45-F0.8-3	10,000 (Not failed)
	T1-S0.3-F0.8-2	10,000 (Not failed)	T1-S0.45-F0.6-1	10,000 (Not failed)
	T1-S0.3-F0.8-3	10,000 (Not failed)	T1-S0.45-F0.6-2	10,000 (Not failed)
	T1-S0.4-F0.8-1	10,000 (Not failed)	T1-S0.45-F0.6-3	10,000 (Not failed)
	T1-S0.4-F0.8-2	10,000 (Not failed)	T1-S0.45-F1.0-1	10,000 (Not failed)
	T1-S0.4-F0.8-3	10,000 (Not failed)	T1-S0.45-F1.0-2	10,000 (Not failed)
	T1-S0.45-F0.8-1	10,000 (Not failed)	T1-S0.45-F1.0-3	10,000 (Not failed)
	T1-S0.45-F0.8-2	10,000 (Not failed)	-	-
Series 2	T2-S0.45-F0.8-1	10,000 (Not failed)	T2-S0.85-F0.8-1	1039
	T2-S0.45-F0.8-2	10,000 (Not failed)	T2-S0.85-F0.8-2	1123
	T2-S0.45-F0.8-3	10,000 (Not failed)	T2-S0.85-F0.8-3	2110
	T2-S0.8-F0.8-1	5708	T2-S0.9-F0.8-1	73
	T2-S0.8-F0.8-2	6324	T2-S0.9-F0.8-2	157
	T2-S0.8-F0.8-3	7407	T2-S0.9-F0.8-3	245
Series 3	T3-S0.8-F0.8-1	7713	T3-S0.85-F0.8-3	2415
	T3-S0.8-F0.8-2	8481	T3-S0.9-F0.8-1	52
	T3-S0.8-F0.8-3	9346	T3-S0.9-F0.8-2	273
	T3-S0.85-F0.8-1	1538	T3-S0.9-F0.8-3	449
	T3-S0.85-F0.8-2	1870	-	-

Note:

T1 – SiMn (SF-FA) in Exposure C for 150 days

T2 – SiMn (SF-FA) in Exposure II for 150 days

T3 – LS (SF-FA) in Exposure II for 150 days
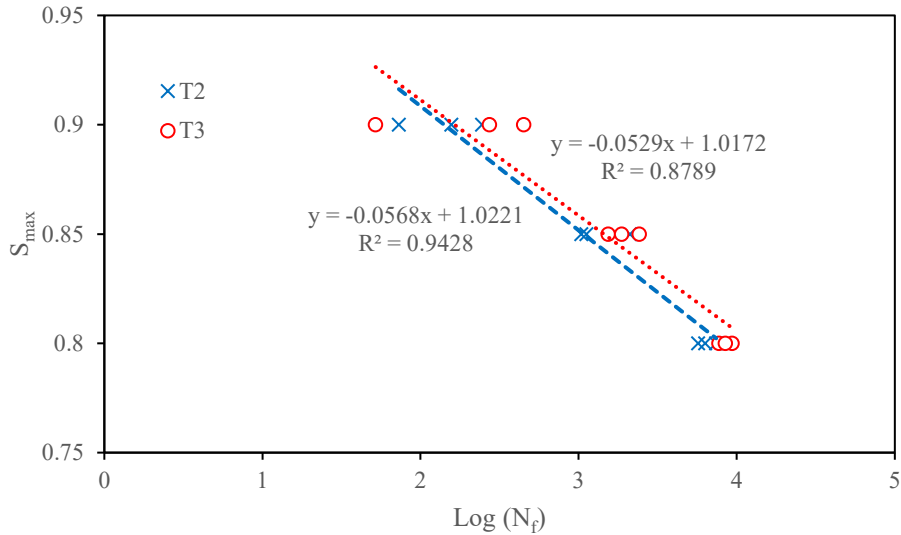
Figure 10: S-N curve of T2 and T3 specimens

3.6.   Deformation under cyclic loading

Concrete undergoes permanent deformation in terms of residual strain as a result of cyclic loading. The residual strain over the fatigue life of T2 and T3 loaded at upper stress level of 80% and loading frequency of 0.8 Hz is shown in Figure 11. In the graph, the strain was normalized with respect to the strain at the last cycle, and the loading cycle is normalized to the fatigue life. The residual strain is divided into three stages, namely initial creeping stage, quasi-linear stage and fatigue stage [38, 39]. The initial creeping stage occurred during 0 to 10% of fatigue life, when the deformation of concrete increased rapidly. This was due to the collapse of void and crack of concrete. In the quasi-linear stage that lasted up to 90% of fatigue life, concrete experienced a low rate of strain increase due to the gradual degradation of inherent defects and the formation of new cracks. The fatigue stage corresponded to a rapid increase in deformation whereby the defects exacerbated and transformed into unstable macro-cracks, leading concrete failure.

472 As shown in Figure 11, T2 specimen generally had a higher residual strain than T3

473 specimen at the initial stage. For example, at the normalized fatigue life of 0.2, the

474 residual strain of T2 was almost two times that of T3. This indicated that T2 had more

475 inherent defects and was weaker than T3. The SiMn slag aggregate used in T2 concrete

476 was flaky and had a relatively smooth surface compared to the limestone aggregate in

477 T3 concrete. As a result, the bonding between SiMn slag aggregate and cement paste

478 was weaker [40]. Furthermore, the SiMn slag aggregate had a lower abrasion resistance

479 than limestone aggregate. Under the dynamic effect of cyclic loading, the development

480 of crack in SiMn slag aggregate was faster than that in the limestone aggregate,

481 contributing to larger deformation. Wu and Jin [36] also found that the concrete

482 containing demolished concrete lump (DCL) aggregate had a higher residual strain due

483 to its weaker mechanical property.

484 Figure 12 presents the average residual displacement of intact specimens after 10,000

485 loading cycles. The residual displacement increased as the upper stress level (S_{max})

486 increased. The residual displacement of T1-S0.4-F0.8 and T1-S0.45-F0.8 was

487 respectively 24.8% and 54.4% higher than that of T1-S0.3-F0.8. The increase in

488 displacement with respect to the upper stress level was not linear. According to Yang

489 et al. [41], the stress-strain relationship of concrete became non-linear when the stress

490 level exceeded 40% of the compressive strength. By comparing T1-S0.45-F0.6, T1-

491 S0.45-F0.8 and T1-S0.45-F1.0, the residual displacement increased with the decrease

492 in loading frequency. At a lower loading frequency, the loading on concrete had to be

493 sustained for a longer period time, resulting in a greater creeping effect of concrete. Wu

494 and Jin [36] reported a rate-dependent property of concrete when the loading frequency

495 was below 1.17 Hz. As for the effects of sulphate attack and WDA, the residual

496 displacement of T2-S0.45-F0.8 was 49.7% higher than that of T1-S0.45-F0.8. T2-

497 S0.45-F0.8 was exposed to 150 days of WDA in 20% Na_2SO_4 solution (Exposure II)

498 and T1-S0.45-F0.8 was fully immersed in tap water for the same period (Exposure C).

499 The sulphate attack and WDA weakened the concrete due to the formation of expansive

500 products and the dissolution of cement hydrate, which softened the concrete. As such,

501 the deteriorated concrete experienced a more significant deformation.

502
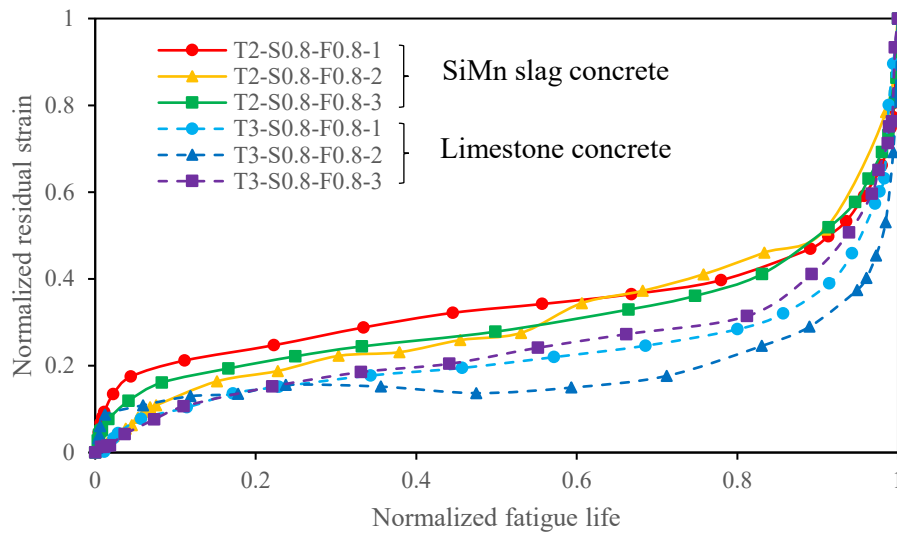
Figure 11: Normalized residual strain of concrete against fatigue life

504

505
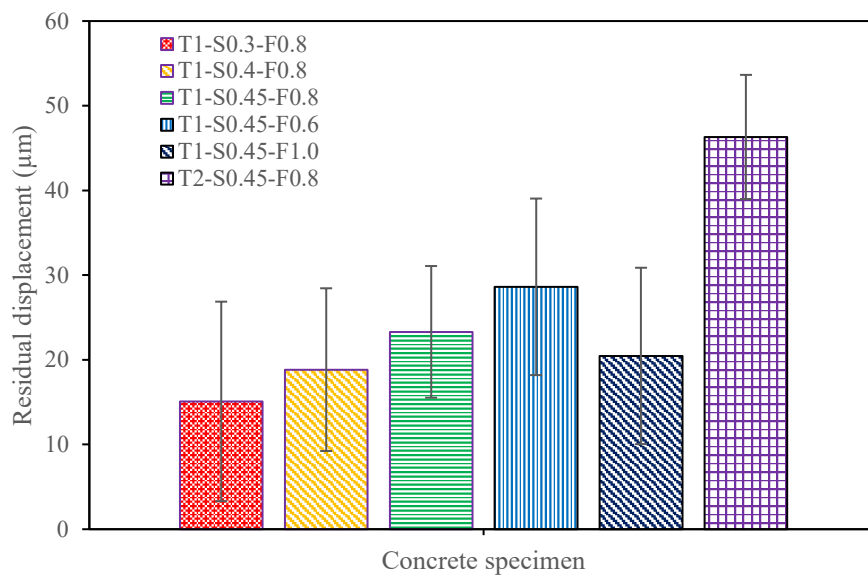
Figure 12: Residual displacement of intact specimen after 10,000 loading cycles

507

3.7.   Modulus of elasticity under cyclic loading

The modulus of elasticity of T2 and T3 is also plotted against the fatigue life as shown

in Figure 13. The elasticity of concrete was normalized to the respective initial elasticity

(E_o) and the loading cycle was normalized to the fatigue life. The change in elasticity

of all concrete specimens was divided into three stages. All specimens experienced a

rapid-stiffening stage, followed by a constant-stiffening stage and, eventually, a rapid-

softening stage. Similar to the residual strain, the three-stage evolution of elasticity

occurred at 0%–10%, 10%–90% and 90–100% of fatigue life, respectively. During the

rapid-stiffening stage, concrete experienced an increase in modulus of elasticity by up

to 9% of its initial value. The finding was slightly different from that presented in

previous studies. For instance, Wu and Jin [36] and Cachim et al. [42] did not notice

any increase in elasticity of concrete during the cyclic loading. In contrast, the concrete

experienced three stages of decrease in elasticity in their works. This was due to the use

of cube specimens in this investigation, which were less slender and stiffer than

cylindrical specimens. In this study, the increased modulus of elasticity was due to the

closing of pores, which made the concrete denser and more compact. The elasticity of

concrete improved further but at a lower rate during the constant-stiffening stage. The

defect developed at this stage, such as micro-crack, had negligible effect on the

robustness of concrete. During the rapid-softening stage, the modulus of elasticity

decreased rapidly, with the largest reduction of 17.4% in T2-S0.8-F0.8-3. The

degradation of stiffness was attributed to the development of macro-cracks, which

ultimately led to concrete failure.

As shown in Figure 13, limestone concrete, T3 experienced a greater increase in elasticity at the initial stage and a smaller decrease in elasticity at the later stage compared to SiMn slag concrete, T2. At 10% of fatigue life, T3 had the highest E/E_o of 1.09 compared to 1.06 exhibited by T2. At a normalized fatigue life of 1, the lowest E/E_o value was 0.826 for T2 and 0.936 for T3. The higher stiffness of T3 was due to its higher resistance to cyclic loading than T2 concrete. T3 concrete was made of stronger limestone aggregate that had a higher abrasion resistance than the SiMn slag aggregate in T2. Besides, the SiMn slag aggregate had a smoother surface than the limestone aggregate, which affected its bonding with cement paste. Consequently, T2 concrete suffered a greater decrease in elasticity during failure.
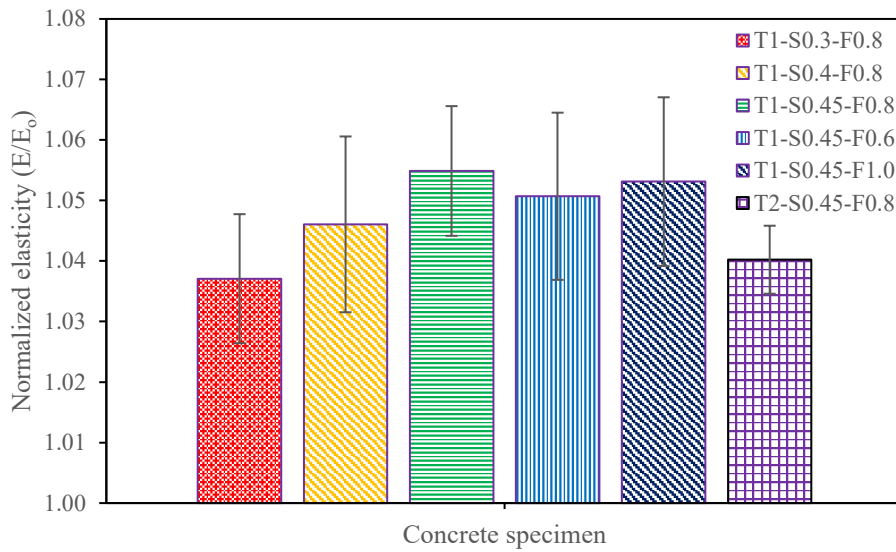
The normalized modulus of elasticity for all intact specimens after 10,000 cycles of loading was determined as shown in Figure 14. The elasticity of all the specimens was higher than their respective initial elasticity (E_o), indicating that concrete failure was not imminent. The increase in the upper stress level caused a greater stiffening effect on concrete. Compared to T1-S0.3-F0.8, the increase in elasticity of T1-S0.4-F0.8 and T1-S0.45-F0.8 was 0.9% and 1.8% higher respectively. This was because more concrete pores were closed at a higher stress level. Besides, the results showed that the loading frequency ranged from 0.6 Hz to 1.0 Hz did not have noticeable effect on the elasticity of concrete. T1-S0.45-F0.6, T1-S0.45-F0.8 and T1-S0.45-F1.0 had similar normalized elasticity values of 1.051, 1.055 and 1.053 respectively. After 150 days of exposure to WDA in 20% Na_2SO_4 solution (Exposure II), T2-S0.45-F0.8 had normalized elasticity of 1.040. This value was lower than the normalized elasticity of 1.055 for T1-S0.45-F0.8 that was fully immersed in tap water (Exposure C). The sulphate attack and WDA deteriorated the mechanical property, resulting in concrete softening and loss of elastic modulus.
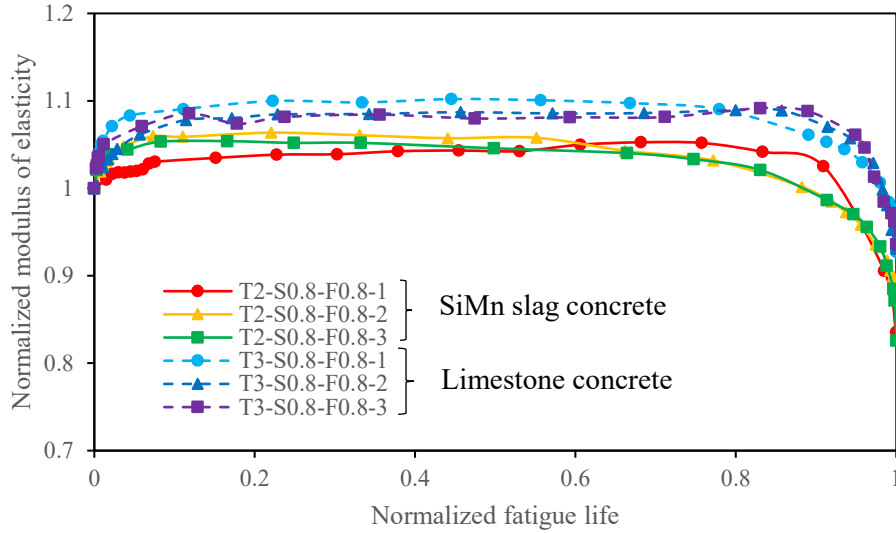
Figure 13: Normalized modulus of elasticity of concrete against fatigue life

Figure 14: Normalized modulus of elasticity of intact specimen after 10,000 loading cycles

3.8.   Compressive strength after cyclic loading

After 10,000 loading cycles, six sets of intact specimens were statically loaded in order

to determine their compressive strength. The compressive strength of these specimens

is shown in Table 8. The compressive strength of concrete after cyclic loading ($f_{c,after}$)
was between 0.98 and 1.05 times their respective original strength (f_c). The $f_{c,after}$ of
concrete was generally higher than f_c except for T1-S0.3-F0.8. The increase in strength
was attributed to the improved stiffness caused by the closing of concrete pores after
the cyclic loading. This finding was consistent with that of Wu and Jin [36], who
discovered the compressive strength of concrete increased by 6% to 16% after 1.5
million loading cycles. As for the reduced compressive strength of T1-S0.3-F0.8, this
could be ascribed to the inherent defects of the concrete that caused the variance in test
results. Furthermore, cyclic loading at S_{max} of 0.3 might not result in permanent closing
of pore, as the concrete was still within elastic range [41].

Table 8: Compressive strength of intact specimens after cyclic loading

Specimen	Original strength, f_c (MPa)	Strength after cyclic loading, $f_{c,after}$ (MPa)	Standard deviation of $f_{c,after}$ (MPa)	$f_{c,after}/f_c$
T1-S0.3-F0.8	91.37	89.48	0.94	0.98
T1-S0.4-F0.8		92.73	1.01	1.01
T1-S0.45-F0.8		93.65	0.85	1.02
T1-S0.45-F0.6		93.11	0.48	1.02
T1-S0.45-F1.0		92.16	0.97	1.01
T2-S0.45-F0.8	40.64	42.52	2.13	1.05

4. Proposed improvement of concrete performance

The previous section demonstrated that the combined mechanisms of sulphate attack,
WDA and cyclic loading had deteriorated the performance of concrete. This will
inevitably result in higher life-cycle cost as a result of the increased maintenance and
repair work in real-world application. The following section discusses on the potential
methods for improving the performance of concrete exposed to this harsh environment.

4.1.   Sulphate-resisting cement

584   The main cause of concrete distress due to external sulphate attack is the formation of

585   expansive products such as ettringite and gypsum. In concrete, calcium hydroxide (CH),

586   tri-calcium aluminate (C_3A) and monosulphate hydrate (C_4ASH_{12}) can react with

587   external sulphate (S) to form ettringite ($C_6AS_3H_{32}$) and gypsum (CSH_2), as shown in

588   Equation 5 to Equation 7 [43].

$$CH + S + 2H_2O \rightarrow CSH_2 + 2OH \qquad\qquad \text{Equation 5}$$

$$C_3A + 3S + 3CH + 32H_2O \rightarrow C_6AS_3H_{32} + 6OH \qquad\qquad \text{Equation 6}$$

$$3C_4ASH_{12} + 3S \rightarrow 2C_6AS_3H_{32} + 2Al(OH)_3 \qquad\qquad \text{Equation 7}$$
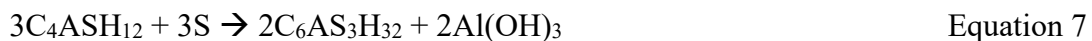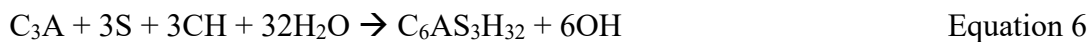
589   The monosulphate hydrate (C_4ASH_{12}) in Equation 7 is also produced from tri-calcium

590   aluminate (C_3A), particularly during the later stage of hydration. In this context, C_3A is

591   the main component of cement that initiates the sulphate attack in concrete. Therefore,

592   one of the strategies for combating sulphate attack is to limit the C_3A content in cement.

593   ASTM C150 [44] specifies the use of Type II and Type V cement as sulphate-resisting

594   (SR) cement for concrete exposed to sulphate attack. However, the low C_3A content in

595   SR cement may have an adverse effect on the strength development of concrete and is

596   hence not recommended for use in marine construction, especially when high early

597   strength is required [45].

598   *4.2.   Supplementary cementitious materials*

599   As illustrated in Equation 5 and Equation 6, CH is also a dominant reactant in concrete

600   that triggers the sulphate attack. As a result, partial replacement of cement with

601   supplementary cementitious materials (SCM) is another method of minimizing the

602   concrete damage caused by sulphate attack. This is because pozzolanic reaction of SCM,

603 such as ground granulated blast-furnace slag, fly ash, metakaolin and silica fume, can

604 consume the CH content, minimizing calcium leaching to produce ettringite and

605 gypsum in concrete [46]. The use of SCM is more advantageous in the long terms since

606 the pozzolanic reaction produces more calcium silicate hydrate (C-S-H), which

607 improves the mechanical performance of concrete in counteracting the sulphate-attack

608 expansion. In addition, the pozzolanic reaction of SCM also enhances and refines the

609 pore structure of hardened cementitious matrix, lowering the concrete permeability to

610 external sulphate [47]. Besides, partially replacing cement with SCM might dilute the

611 clinker compositions, which proportionately reduces the C_3A level in concrete for the

612 sulphate attack reaction. In summary, the incorporation of SCM can be an effective

613 sulphate attack mitigation approach, particularly when high strength and durable

614 concrete is required for maritime applications.

615 *4.3.   Fibre-reinforced concrete*

616 Fibre-reinforced concrete (FRC) is a type of concrete that comprises fibrous materials

617 such as basalt fibre, glass fibre, polymer fibre and steel fibre, and generally has better

618 cracking resistance and post-cracking performance [48]. Therefore, the FRC exhibits

619 improved fatigue resistance, since the fatigue failure of concrete is associated with the

620 growth of crack and irreversible strain. The presence of fibre provides a bridging effect

621 within the cementitious matrix, and the action of fibre pull-out helps to dissipate energy,

622 which can prevent the development of crack [17]. Furthermore, the incorporation of

623 fibre can also improve the mechanical properties of concrete, increasing its load

624 carrying capacity and fatigue resistance [49]. Dong et al. [48] showed that the FRC had

625 a denser microstructure with an improved interfacial transition zone as the pores were

626 filled by the embedded fibre in cementitious matrix. Based on the findings, FRC may

627 be more resistant to sulphate attack due to its better mechanical performance, but further

628 investigation is required to confirm this.

629 **5. Conclusions**

630 This experimental study investigated the compressive fatigue behavior of concrete

631 exposed to sulphate attack and wetting-drying action (WDA). The sulphate penetration

632 profile as well as mass and volume changes of concrete were determined. The study

633 compared the performance of SiMn slag and limestone concrete. Based on the

634 experimental results, the following conclusions are drawn.

635 1. Sulphate (SO_4^{2-}) ion could penetrate into concrete up to 20 mm depth. The

636   maximum SO_4^{2-} ion content of 1.72%–2.58% was found at the penetration depth of

637   0–5 mm. Sulphate penetration was greater in concrete exposed to WDA than that

638   exposed to full immersion.

639 2. Concrete experienced a mass gain of 0.04%–0.43% during the exposure period 0–

640   90 days, but a mass loss of 0.05%–0.49% during 90–150 days.

641 3. Concrete expanded throughout the exposure time with a maximum value ranging

642   between 0.73% and 1.23%.

643 4. Cyclic loading together with sulphate attack and WDA weakened the concrete,

644   causing an increase in residual displacement and a decrease in elastic modulus.

645 5. Cyclic loading test showed that an increase in upper stress level from 30% to 45%

646   of concrete compressive strength increased its residual displacement by 54.4%. A

647   decrease in loading frequency from 1 Hz to 0.6 Hz reduced the residual

648   displacement by 39.9%.

6. After 10,000 loading cycles, intact specimens exhibited a residual displacement of 15.1–46.3 μm. The elastic modulus improved by 1.037–1.055 times. The compressive strength increased by 1.01–1.05 times.

7. The S-N curve of SiMn slag concrete was lower than that of limestone concrete, indicating that SiMn slag concrete had a lower fatigue life. SiMn slag concrete exhibited greater residual strain and stiffness degradation than limestone concrete.

The combined mechanisms of sulphate attack, WDA and cyclic loading resulted in more critical degradation of concrete than if only individual mechanism was involved. In practical engineering application, the synergy between these deterioration mechanisms exists and must be taken into account for the design of maritime structure. Fatigue resistance of concrete structure should also be included as design criteria to ensure its long-term performance.

Reference

[1] Gaythwaite, J.W. *Design of marine facilities for the berthing, mooring, and repair of vessels*. 2004. American Society of Civil Engineers.
[2] Ting, M.Z.Y., K.S. Wong, M.E. Rahman, and S.J. Meheron, *Deterioration of marine concrete exposed to wetting-drying action.* Journal of Cleaner Production, 2020: p. 123383.
[3] Apostolopoulos, C.A., K.F. Koulouris, and A.C. Apostolopoulos, *Correlation of Surface Cracks of Concrete due to Corrosion and Bond Strength (between Steel Bar and Concrete).* Advances in Civil Engineering, 2019. **2019**: p. 343-354.

[4] Samimi, K., S. Kamali-Bernard, and A.A. Maghsoudi, *Durability of self-compacting concrete containing pumice and zeolite against acid attack, carbonation and marine environment.* Construction and Building Materials, 2018. **165**: p. 247-263.

[5] Jiang, L. and D. Niu, *Study of deterioration of concrete exposed to different types of sulfate solutions under drying-wetting cycles.* Construction and Building Materials, 2016. **117**: p. 88-98.

[6] Roziere, E., A. Loukili, R. El Hachem, and F. Grondin, *Durability of concrete exposed to leaching and external sulphate attacks.* Cement and Concrete Research, 2009. **39**(12): p. 1188-1198.

[7] Liu, Z., X. Li, D. Deng, G. De Schutter, and L. Hou, *The role of Ca (OH) 2 in sulfate salt weathering of ordinary concrete.* Construction and Building Materials, 2016. **123**: p. 127-134.

[8] Mota, B., T. Matschei, and K. Scrivener, *The influence of sodium salts and gypsum on alite hydration.* Cement and Concrete Research, 2015. **75**: p. 53-65.

[9] Kunther, W., B. Lothenbach, and K.L. Scrivener, *On the relevance of volume increase for the length changes of mortar bars in sulfate solutions.* Cement and Concrete Research, 2013. **46**: p. 23-29.

[10] Mullauer, W., R.E. Beddoe, and D. Heinz, *Sulfate attack expansion mechanisms.* Cement and concrete research, 2013. **52**: p. 208-215.

[11] Shazali, M.A., M.H. Baluch, and A.H. Al-Gadhib, *Predicting residual strength in unsaturated concrete exposed to sulfate attack.* Journal of Materials in Civil Engineering, 2006. **18**(3): p. 343-354.

[12] Zhongya, Z., J. Xiaoguang, and L. Wei, *Long-term behaviors of concrete under low-concentration sulfate attack subjected to natural variation of environmental climate conditions.* Cement and Concrete Research, 2019. **116**: p. 217-230.

[13] Zhang, J., M. Sun, D. Hou, and Z. Li, *External sulfate attack to reinforced concrete under drying-wetting cycles and loading condition: numerical simulation and experimental validation by ultrasonic array method.* Construction and Building Materials, 2017. **139**: p. 365-373.

[14] Wu, Z., H. Wong, and N. Buenfeld, *Transport properties of concrete after drying-wetting regimes to elucidate the effects of moisture content, hysteresis and microcracking.* Cement and concrete research, 2017. **98**: p. 136-154.

[15] Gao, J., Z. Yu, L. Song, T. Wang, and S. Wei, *Durability of concrete exposed to sulfate attack under flexural loading and drying–wetting cycles.* Construction and Building Materials, 2013. **39**: p. 33-38.

[16] Chen, F., J. Gao, B. Qi, D. Shen, and L. Li, *Degradation progress of concrete subject to combined sulfate-chloride attack under drying-wetting cycles and flexural loading.* Construction and Building Materials, 2017. **151**: p. 164-171.

[17] Lee, M. and B. Barr, *An overview of the fatigue behaviour of plain and fibre reinforced concrete.* Cement and Concrete Composites, 2004. **26**(4): p. 299-305.

[18] Jiang, C., X. Gu, Q. Huang, and W. Zhang, *Deformation of concrete under high-cycle fatigue loads in uniaxial and eccentric compression.* Construction and Building Materials, 2017. **141**: p. 379-392.

[19] *ACI Committee 215. 1997. Considerations for Design of Concrete Structures Subjected to Fatigue Loading (ACI 215R-74). Farmington Hills, MI: American Concrete Institute*.

[20] Liu, F., Z. You, A. Diab, Z. Liu, C. Zhang, and S. Guo, *External sulfate attack on concrete under combined effects of flexural fatigue loading and drying-wetting cycles.* Construction and Building Materials, 2020. **249**: p. 118224.

[21] Yu, D., B. Guan, R. He, R. Xiong, and Z. Liu, *Sulfate attack of Portland cement concrete under dynamic flexural loading: A coupling function.* Construction and Building Materials, 2016. **115**: p. 478-485.

724   [22] Ting, M.Z.Y., K.S. Wong, M.E. Rahman, and M.S. Joo, *Mechanical and durability*
725   *performance of marine sand and seawater concrete incorporating silicomanganese slag as*
726   *coarse aggregate.* Construction and Building Materials, 2020. **254**: p. 119195.
727   [23] Ting, M.Z.Y., K.S. Wong, M.E. Rahman, and M. Selowarajoo, *Prediction model for*
728   *hardened state properties of silica fume and fly ash based seawater concrete incorporating*
729   *silicomanganese slag.* Journal of Building Engineering, 2021. **41**: p. 102356.
730   [24] *ASTM C494, Standard specification for chemical admixtures for concrete*. 2019, American
731   Society for Testing and Materials: West Conshohocken, PA.
732   [25] *ACI Committee 211. 2009. Guide for selecting proportions for high-strength concrete using*
733   *Portland cement and other cementitious material (ACI 211.4R-08)*. American Concrete
734   Institute: Farmington Hills, MI.
735   [26] *ASTM C114, Standard test methods for chemical analysis of hydraulic cement*. 2018,
736   American Society for Testing and Materials: West Conshohocken, PA.
737   [27] *ASTM C1012, Standard test method for length change of hydraulic-cement mortars*
738   *exposed to a sulfate solution*. 2018, American Society for Testing and Materials: West
739   Conshohocken, PA.
740   [28] Qi, B., J. Gao, F. Chen, and D. Shen, *Evaluation of the damage process of recycled*
741   *aggregate concrete under sulfate attack and wetting-drying cycles.* Construction and Building
742   Materials, 2017. **138**: p. 254-262.
743   [29] Zhang, H., T. Ji, and H. Liu, *Performance evolution of the interfacial transition zone (ITZ) in*
744   *recycled aggregate concrete under external sulfate attacks and dry-wet cycling.* Construction
745   and Building Materials, 2019. **229**: p. 116938.
746   [30] Maes, M. and N. De Belie, *Resistance of concrete and mortar against combined attack of*
747   *chloride and sodium sulphate.* Cement and Concrete Composites, 2014. **53**: p. 59-72.
748   [31] Tang, J., H. Cheng, Q. Zhang, W. Chen, and Q. Li, *Development of properties and*
749   *microstructure of concrete with coral reef sand under sulphate attack and drying-wetting*
750   *cycles.* Construction and Building Materials, 2018. **165**: p. 647-654.
751   [32] Qi, B., J. Gao, F. Chen, and D. Shen, *Chloride penetration into recycled aggregate concrete*
752   *subjected to wetting–drying cycles and flexural loading.* Construction and Building Materials,
753   2018. **174**: p. 130-137.
754   [33] Yu, X.T., D. Chen, J.R. Feng, and Y. Zhang, *Behavior of mortar exposed to different exposure*
755   *conditions of sulfate attack.* Ocean Engineering, 2018. **157**: p. 1-12.
756   [34] Del Viso, J., J. Carmona, and G. Ruiz, *Shape and size effects on the compressive strength*
757   *of high-strength concrete.* Cement and Concrete Research, 2008. **38**(3): p. 386-395.
758   [35] Fladr, J. and P. Bily, *Specimen size effect on compressive and flexural strength of high-*
759   *strength fibre-reinforced concrete containing coarse aggregate.* Composites Part B:
760   Engineering, 2018. **138**: p. 77-86.
761   [36] Wu, B. and H. Jin, *Compressive fatigue behavior of compound concrete containing*
762   *demolished concrete lumps.* Construction and Building Materials, 2019. **210**: p. 140-156.
763   [37] Humme, J., C. von der Haar, L. Lohaus, and S. Marx, *Fatigue behaviour of a normal‐*
764   *strength concrete – number of cycles to failure and strain development.* Structural Concrete,
765   2016. **17**(4): p. 637-645.
766   [38] Choi, S.J., J.S. Mun, K.H. Yang, and S.J. Kim, *Compressive fatigue performance of fiber-*
767   *reinforced lightweight concrete with high-volume supplementary cementitious materials.*
768   Cement and Concrete Composites, 2016. **73**: p. 89-97.
769   [39] Medeiros, A., X. Zhang, G. Ruiz, C.Y. Rena, and M.d.S.L. Velasco, *Effect of the loading*
770   *frequency on the compressive fatigue behavior of plain and fiber reinforced concrete.*
771   International Journal of Fatigue, 2015. **70**: p. 342-350.
772   [40] Kazjonovs, J., D. Bajare, and A. Korjakins, *Designing of high density concrete by using steel*
773   *treatment waste.* The 10th International Conference Modern building materials, structures
774   and techniques, 2010: p. 138-142.

775   [41] Yang, K.H., J.H. Mun, M.S. Cho, and T.H. Kang, *Stress-strain model for various unconfined*
776   *concretes in compression.* ACI Structural Journal, 2014. **111**(4): p. 819.
777   [42] Cachim, P.B., J.A. Figueiras, and P.A. Pereira, *Fatigue behavior of fiber-reinforced concrete*
778   *in compression.* Cement and concrete composites, 2002. **24**(2): p. 211-217.
779   [43] Ikumi, T. and I. Segura, *Numerical assessment of external sulfate attack in concrete*
780   *structures. A review.* Cement and Concrete Research, 2019. **121**: p. 91-105.
781   [44] *ASTM C150, Standard specification of Portland cement*. 2012, American Society for
782   Testing and Materials: West Conshohocken, PA.
783   [45] Irassar, E., M. Gonzalez, and V. Rahhal, *Sulphate resistance of type V cements with*
784   *limestone filler and natural pozzolana.* Cement and Concrete Composites, 2000. **22**(5): p. 361-
785   368.
786   [46] Atahan, H. and D. Dikme, *Use of mineral admixtures for enhanced resistance against*
787   *sulfate attack.* Construction and Building Materials, 2011. **25**(8): p. 3450-3457.
788   [47] Elahi, M.M.A., C.R. Shearer, A.N.R. Reza, A.K. Saha, M.N.N. Khan, M.M. Hossain, and P.K.
789   Sarker, *Improving the sulfate attack resistance of concrete by using supplementary*
790   *cementitious materials (SCMs): A review.* Construction and Building Materials, 2021. **281**: p.
791   122628.
792   [48] Dong, J., Q. Wang, and Z. Guan, *Material properties of basalt fibre reinforced concrete*
793   *made with recycled earthquake waste.* Construction and Building Materials, 2017. **130**: p. 241-
794   251.
795   [49] Chen, M., H. Zhong, and M. Zhang, *Flexural fatigue behaviour of recycled tyre polymer*
796   *fibre reinforced concrete.* Cement and Concrete Composites, 2020. **105**: p. 103441.
797